Title
Human 15-LOX-1 active site mutations alter inhibitor binding and decrease potency.

Authors
Armstrong, Michelle
van Hoorebeke, Christopher
Horn, Thomas
et al.

HUMAN 15-LOX-1 ACTIVE SITE MUTATIONS ALTER INHIBITOR BINDING AND DECREASE POTENCY

Michelle Armstrong[1], **Christopher van Hoorebeke**[1], **Thomas Horn**[1,&], **Joshua Deschamps**[1], **J. Cody Freedman**[1], **Chakrapani Kalyanaraman**[2], **Matthew P. Jacobson**[2], and **Theodore Holman**[1,*]

[1]Department of Chemistry and Biochemistry, University of California Santa Cruz, Santa Cruz, CA 95064, United States

[2]Department of Pharmaceutical Chemistry, School of Pharmacy, University of California San Francisco, San Francisco, California, 94143, United States
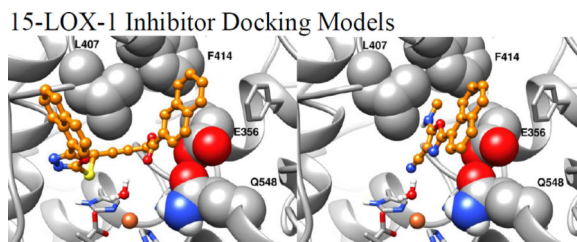
Abstract

Human 15-Lipoxygenase-1 (h15-LOX-1 or h12/15-LOX) reacts with polyunsaturated fatty acids and produces bioactive lipid derivatives that are implicated in many important human diseases. One such disease is stroke, which is the fifth leading cause of death and the first leading cause of disability in America. The discovery of h15-LOX-1 inhibitors could potentially lead to novel therapeutics in the treatment of stroke, however, little is known about the inhibitor/active site interaction. This study utilizes site-directed mutagenesis, guided in part by molecular modeling, to gain a better structural understanding of inhibitor interactions within the active site. We have generated eight mutants (R402L, R404L, F414I, F414W, E356Q, Q547L, L407A, I417A) of h15-LOX-1 to determine whether these active site residues interact with two h15-LOX-1 inhibitors, **ML351** and an **ML094** derivative, compound **18**. IC_{50} values and steady-state inhibition kinetics were determined for the eight mutants, with four of the mutants affecting inhibitor potency relative to wild type h15-LOX-1 (F414I, F414W, E356Q and L407A). The data indicate that **ML351** and compound **18,** bind in a similar manner in the active site to an aromatic pocket close to F414 but have subtle differences in their specific binding modes. This information establishes the binding mode for **ML094** and **ML351** and will be leveraged to develop next-generation inhibitors.

Graphical Abstract

15-LOX-1 Inhibitor Docking Models

Keywords

human; 15-lipoxygenase-1; mutagenesis; inhibitor; docking

Introduction

Human reticulocyte 15-lipoxygenase-1 (h15-LOX-1 or h12/15-LOX) has been linked to inflammation, cardiovascular disease, carcinogenesis/metastasis, and metabolic disorders/ neurological disorders.[1–13] One disorder in which h15-LOX-1 has been strongly associated with is stroke.[13–15] Stroke is the fifth leading cause of death and the leading cause of disability in the United States, but the only FDA approved drug currently available is tissue plasminogen activator (tPA). Therefore, inhibitors targeting h15-LOX-1 with low nano-molar potency and good activity in neuronal cells could be possible treatments of stroke.

h15-LOX-1 catalyzes the dioxygenation of various polyunsaturated fatty acids (PUFAs), both as the free fatty acid and as the phospholipid linked fatty acid. Over the years, a variety of inhibitors have been discovered which target h15-LOX-1. Bristol-Myers Squibb's tryptamine sulfonamide exhibited a potency of 21 nM.[16] A family of pyrazole-based sulfonamides and sulfamides were reported to have potencies of about 1 nM, while a class of imidazole-based derivatives had potencies around 75 nM.[17,18] Pelcman *et. al.* identified BLX-2477 (N-(2-chloro-4-fluorophenyl)triazole-4-carboxamide) with a potency of 99 nM, but the inhibitor exhibited adverse off-target effects in mini-pigs and was not potent against the dog or rat LOX orthologs.[19,20] Eleftheriadis *et. al.* published a novel family of 6-benzyloxysalicylate inhibitors with modest potency (7100 nM) against h15-LOX-1.[21] Our laboratories have discovered two inhibitor scaffolds that target h15-LOX-1, **ML094** (4-(5-(Naphthalen-1-yl)-1,3,4-oxadiazol-2-ylthio)but-2-ynylthiophene-2-carboxylate), and **ML351** (5-(methylamino)-2-(naphthalene-1-yl)oxazole-4-carbonitrile).[22,23] The structure of **ML094** is similar to **ML351** (Table 1) in that they both contain a naphthalene moiety attached to a 5-member heterocycle, but **ML094** differs in that it has a longer hydrophobic arm, opposite the naphthalene group. **ML094** exhibits low nano-molar potency *in vitro* but has no activity *in vivo*, possibly due to the cellular lability of the ester moiety.[22] On the other hand, **ML351** has sub-micromolar potency and exhibits *in vivo* activity in mice.[24] Due to their similar structures, we have assumed both **ML094** and **ML351** bind to similar sites on h15-LOX-1, however, the lack of a co-crystal structure of either inhibitor with h15-LOX-1 has made the improvement of these two inhibitor series challenging.

The structure of the rabbit homologue of h15-LOX-1 (r15-LOX) has been solved with an inhibitor bound to the active site (Figure 1a).[25,26] The inhibitor, RS75091 (Table 1), weakly

coordinates to the active site iron and interacts with the deep pocket of the active site. Specifically, the phenyl ring of RS75091 points toward the Phe415/Phe353 (Phe414/Phe352 in h15-LOX-1), while the carboxylic acid and alkyl chain point back into the cavity. It is important to note that the unit cell contains two proteins, labeled "closed" and "open" structures. The closed structure is defined by having the inhibitor bound to the active site, while the open structure does not have the inhibitor bound (PDB file: 2P0M, chain A is the open structure and chain B is the closed structure). This difference in structure due to inhibitor binding suggests plasticity in the active site and presents challenges for structure-based drug design.

Previous studies have investigated specific amino acids in the active site of h15-LOX-1 through mutagenesis to better understand the residues involved in substrate binding. Gan *et. al.* investigated three active site residues, R402, F414, and L407.[27] They mutated R402 to a leucine, which led to a change in positional specificity of catalysis, changing the 15-HpETE/ 12-HpETE ratio from 9:1 to 4:1 and a dramatic decrease in the rate of substrate capture (k_{cat}/K_M).[27] These data support the hypothesis that the fatty acid substrate penetrates the active site with the methyl terminus end first, allowing the carboxyl end of the fatty acid to interact with R402 at the entrance of the substrate channel. Mutation of F414, an aromatic residue that resides near the catalytic iron, also affected proper alignment of substrate in the active site. This residue is proposed to participate in a π-π interaction with the ^{11}-double bond of arachidonic acid and ^{9}-double bond of linoleic acid.[27] L407, thought to control the entrance of the narrow pocket of the methyl-end binding region of the substrate, did not affect substrate binding significantly, despite the fact that L407 is conserved in all of the lipoxygenases. Interestingly, Klinman *et. al.* mutated the homologous residue to L407 in soybean lipoxygenase (s15-LOX-1), L546, to an alanine and found that the A546 mutant made 10% more 9R-HpODE, a product resulting from oxygen attacking on the same face as H-atom abstraction.[28] This data suggests that this residue could control the regiochemistry of oxygenation and participate in guiding oxygen to its proper location.[28] Two catalytic residues, I417 and F352, which reside at the end of the narrow methyl-end binding region, restrict the penetration of the fatty acid methyl tail, and generate 15-HpETE as the primary product, with a 9:1 ratio of 15-HpETE/ 12-HpETE.[27–30] The I417A or F352L mutants allow AA to bind deeper into the active site, resulting in the C10 hydrogen atom to be abstracted, and an increase in 12-HpETE formation (1:15 ratio of 15-HpETE/ 12-HpETE).[31] Finally, E356 and Q547 (E357 and Q548 in r15-LOX) participate in a hydrogen-bonding network in the active site, which may provide a structural link between substrate binding and iron coordination.[25]

In the current work, we have mutated eight active site residues, based on the above observations and molecular modeling of inhibitor binding, and have determined their effects on the IC$_{50}$ and steady state inhibition parameters of **ML351 and** an **ML094** derivative, compound **18** (Table 1).

Experimental Procedures

Chemicals

All commercial fattyacids were purchased from Nu Chek Prep, Inc. (MN, USA). All other chemicals were reagent grade or better and were used without further purification.

Site-directed Mutagenesis

All mutations of the human 15-LOX-1 enzyme (R402L, R404L, E356Q, Q547L, F414I, F414W, L407A, I417A, F352L) were performed using the QuikChange® II XL site-directed mutagenesis kit from Agilent Technologies (CA, USA), following the instructions of the manufacturer's protocol. The mutation was confirmed by sequencing the LOX insert in the pFastBac1 shuttle vector (Operon, gene with Operon (KY, USA).

Protein Expression

The h15-LOX-1 enzymes used in this publication were expressed and purified as previously published.[32] All mutants, (R402L, R404L, F414I, F414W, E356Q, Q547L, I417A, L407A), were expressed as N-terminal His6-tagged fusion proteins and were purified via cation exchange affinity chromatography, using Bio-Rad Macro-Prep High S cation exchange resins, or with an IMAC column, depending on the mutation. The protein purity was evaluated by SDS-PAGE analysis and was found to be greater than 90% for all the enzymes.

Determination of Iron Content using ICP-MS

The iron content of the mutants were determined relative to WT h15-LOX-1 using a Thermo Element XR inductively coupled plasma mass spectrometer (ICP-MS) and cobalt (EDTA) as an internal standard. Iron concentrations were compared to standard iron solutions. All kinetic data were normalized to the iron content. The protein concentration was determined using the Bradford assay, with bovine serum albumin (BSA) as the protein standard.

Lipoxygenase UV-Vis-based IC$_{50}$ Assay

The inhibition potencies were determined by following the formation of the conjugated diene products, 15-HpETE ($\varepsilon = 27,000$ M^{-1}cm^{-1}) or 13-HpODE ($\varepsilon = 23,000$ M^{-1}cm^{-1}), at 234 nm with a Perkin-Elmer Lambda 40 UV/Vis spectrophotometer at five inhibitor concentrations (each concentration in triplicate). All reaction mixtures were 2 mL in volume and constantly stirred using a magnetic stir bar at room temperature (23°C) with the appropriate amount of LOX isozyme (h15-LOX-1 (~ 30 nM); F414I (~ 150 nM); F414W (~ 67 nM); E356Q (~ 100 nM); Q547L (~ 80 nM); R402L (~ 112 nM); R404L (~ 130 nM); I417A (~ 60 nM); L407A (~ 100 nM)). All reactions were carried out in 25 mM HEPES buffer (pH 7.5), 0.01% Triton X-100 and 10 μM AA or LA. The concentration of AA or LA was quantitated by enzymatic reaction with s15-LOX-1 and allowing the reaction to go to completion. IC$_{50}$ values were obtained by determining the enzymatic rate at five inhibitor concentrations and plotting them against inhibitor concentration, followed by a hyperbolic saturation curve fit. The data used for the saturation curve fits were performed in duplicate or triplicate, depending on the quality of the data. The IC$_{50}$ values of the mutants were

compared to the IC$_{50}$ values of the wild-type h15-LOX-1 on the same day, to determine whether the mutation had an effect on inhibitor potency.

Steady-State Kinetics

The h15-LOX-1 and mutant rates were determined the same way as the UV-Vis-Based Assay. Reactions were initiated by adding the LOX enzyme to a constantly stirring 2 mL reaction mixture containing 1 μM – 20 μM AA or LA in 25 mM HEPES buffer (pH 7.5), in the presence of 0.01% Triton X-100. Kinetic data were obtained by recording initial enzymatic rates at each substrate concentration and subsequently fitting them to the Henri-Michaelis-Menten equation, using KaleidaGraph (Synergy) to determine k_{cat} and k_{cat}/K_M values.

Steady-State Inhibition Kinetics

h15-LOX-1 and mutant rates were determined the same way as the UV-Vis-Based Assay. Reactions were initiated by adding the LOX isozyme to a constantly stirring 2 mL reaction mixture containing 1 μM – 20 μM AA or LA in 25 mM HEPES buffer (pH 7.5), 0.01% Triton X-100. Kinetic data were obtained by recording initial enzymatic rates, at varied inhibitor concentrations, and subsequently fitting them to the Henri-Michaelis-Menten equation, using KaleidaGraph (Synergy) to determine the microscopic rate constants, k_{cat} (sec^{-1}) and k_{cat}/K_M (sec^{-1}μM^{-1}). These rate constants were subsequently replotted as 1/k_{cat} or K_M/k_{cat} versus inhibitor concentration, to yield K_{iu} and K_{ic}, respectively, which are defined as the equilibrium constant of dissociation from the secondary and catalytic sites. The primary data was also plotted in the Dixon format, graphing 1/v vs. [I] μM at the chosen substrate concentrations. From the Dixon plots, the slope at each substrate concentration was extracted and plotted against 1/[S] μM to produce the Dixon parameters, K_{iu} and K_{ic}.

Computational Methods

A homology model of human 15-Lipoxygenase-1 (h15-LOX-1) sequence (UniProt accession P16050) was built from the closed inhibitor bound structure of rabbit reticulocyte 15-LOX (pdb ID 2P0M, chain B, sequence identity 81%), using the software PRIME (Schrodinger Inc). Both metal ion (Fe^{2+}) and co-crystallized inhibitor were included during homology modeling. In addition, we have also copied a water molecule that coordinates to the metal ion in the h15-LOX-2 structure (pdb ID; 4nre). The model was energy minimized using Protein Preparation Wizard (Schrodinger Inc).[33] After energy minimization the inhibitor was separated, leaving the protein, Fe^{2+} ion and a water molecule as a separate entry in the Maestro project table (Maestro v97012, Schrodinger Inc).[33] We copied this protein model into multiple entries and in each entry we made one specific mutation (viz. F414I, F414W, L407A, E356Q and Q547L) using Maestro's Edit/Build panel (Schrodinger Inc). After making the virtual mutation, the side chain of the mutated residue was optimized using PRIME side chain prediction module (Schrodinger Inc).[33] Once a low energy side chain conformation was found, the resulting structure was used in our subsequent docking studies. We used the previously separated inhibitor coordinates to define the binding site for docking to the wild-type (WT) and mutant h15-LOX-1 enzymes. Inhibitor **18** of the **ML094** series and **ML351** were manually built using Maestro's Edit/Build panel and energy

minimized using LigPrep software (LigPrep v36017, Schrodinger Inc).[33] In addition to adding hydrogens, LigPrep also expands protonation states and chiralities of the inhibitors. For both inhibitors only one final structure was obtained after LigPrep energy minimization. Docking software Glide (Glide v58515, Schrodinger Inc) was used for flexible-ligand rigid-receptor docking. Glide extra precision scoring function (Glide-XP) was used to obtain the docking pose and score for each inhibitor.[33] We performed the docking calculation for both WT and mutant h15-LOX-1 enzymes. Both the metal ion (Fe^{2+}) and the water molecule were included during all docking calculations.

Results and Discussion

Molecular Modeling Predictions of ML351 and Compound 18 Binding Modes

To develop hypotheses concerning their binding modes, inhibitors **ML351** and compound **18** were computationally docked to a model of WT h15-LOX-1 (subsequently referred to as WT), using Glide XP. The docking scores are presented in Table 2, and the predicted binding poses in Figure 1.

Compound **18** is pseudo-symmetrical and binds in a U-shape binding mode (Figure 1b), similar to the ligand binding mode observed in porcine leukocyte 12-LOX and human epithelial 15-LOX-2 co-crystal structures.[34,35] The acetylene group in the linker region is in the vicinity of the metal ion and the water molecule, which makes a hydrogen bond donor interaction with the ester oxygen of the inhibitor (2.3Å).

ML351 is much smaller than **18** but the naphthalene rings of both inhibitors bind deeply in the hydrophobic pocket created by F352 and F414 (Figure 1d). This binding mode is very similar to that of the aromatic group in RS75091 in its co-crystal structure with the rabbit homolog (pdb id 2P0M, chain B), suggesting a common aromatic binding site (Figure 1c). Docking poses of two previously reported inhibitors also show that the phenyl ring of the inhibitors bound in the same aromatic binding site.[36,37] However, when a larger ligand with a salicylate moiety, N296-Eleftheriadis, was docked to the WT h15-LOX1 model, the hydroxybenzoate ring (salicylate) flips and a long aliphatic chain binds in the aromatic binding site. This observation highlights the hydrophobic nature of the aromatic binding site.[21] The oxazole ring in **ML351** is a bioisostere of the ester group and its hydrogen bond acceptor nitrogen is 2.8 Å from the hydrogen atom of the water molecule. However, unlike the ester group in **18**, the oxazole ring in **ML351** is geometrically constrained due to substitutions at all 3 carbons.

To assess the predicted binding modes, with the ultimate goal of further optimizing the inhibitors, we identified side chains in the active site that are predicted to form key interactions with the inhibitors; some of the resulting mutations have been examined in other contexts previously, as described in the Introduction. We identified residues that were within 5Å to the docked inhibitor's heavy atoms and made hydrogen bonding and hydrophobic interactions with the inhibitor. F414 was predicted to form key hydrophobic contacts with both inhibitors, suggesting that mutations to it would perturb binding of both ligands. Two mutations were chosen, F414I, which removes the aromatic character, and F414W, which retains the aromatic character but would be expected to reduce the size of the hydrophobic

pocket. We created models of these mutants of h15-LOX-1 and re-docked both inhibitors (Table 2 and Figure 2). Interestingly, only F414I was predicted to negatively impact binding of **ML351** (based on worse docking score), whereas F414W was predicted to more negatively impact the binding of compound **18**. The difference in the predicted behavior appears to be due to the size of the inhibitors. The smaller **ML351** can, in some cases, reorient itself to find other (predicted) favorable binding modes, while the larger compound **18** is much more restricted.

Mutation of L407, specifically L407A, was likewise predicted to have differing impacts on **ML351** and compound **18**. L407 makes fewer interactions with **ML351** than with compound **18**. Due to the U-shaped binding mode of compound **18** (Figure 1b), L407 is predicted to play a particularly central role, binding in the middle of the "U" and forming favorable interactions with both aromatic groups of compound **18**. As such, L407A is predicted to negatively impact binding affinity of compound **18**, which docks in a completely different manner than with WT.

Predicted binding modes of **ML351** were significantly different from the WT binding mode upon F414I, F414W, and L407A mutations; similarly, the L407A and E356Q mutations were predicted to significantly change the mode of binding of compound **18**, respectively. To ensure that these predictions are not an artifact of the docking procedure, in which we predicted the side chain rotamer of the mutated residue with no ligand present, we performed an alternate calculation in which we forced the compounds to the wild-type binding mode, predicted side chains of the mutated residues with the ligands present, and evaluated the docking score, using "score-in-place" docking mode (i.e., not sampling inhibitor conformations). In Table 2, docking scores (XP score-in-place) from this calculation are reported. Due to the pseudo-symmetrical nature of compound 18, the docking scores are remarkably similar even when the binding pose is 180° flipped, because very similar hydrophobic and hydrophilic interactions are retained. For **ML351**, the docking scores for the F414W and L407A mutations are significantly worse when the compound is forced to retain the binding mode predicted for WT, supporting the suggestion that the mutation will result in significant changes in **ML351** binding mode. The results of ML351 in the F414I mutation are more ambiguous, with similar docking scores when the compound adopts two very different conformations.

Determination of Steady-State Substrate Kinetics

The steady-state substrate kinetic experiments for F414W, E356Q, Q547L, R402L, R404L, and L407A were executed using AA as the substrate, while LA was required for F414I kinetics, due to rapid product degradation of AA relative to WT. Gratifyingly, the steady-state substrate kinetic parameters for all the mutants (k_{cat}, K_M and k_{cat}/K_M) agreed well with those seen in the literature and were within 50% of the WT values (Table 3).[27] The data confirms the hypothesis that these active site mutations do not alter the WT kinetics significantly and represent relatively minor perturbations to the active site.

Determination of Mutation Effects on Inhibitor Potency

To determine the effect of a specific mutation on inhibitor potency, **ML351** and compound **18**, an **ML094** derivative (Table 3), were screened against active site mutants (R402L, R404L, F414I, F414W, E356Q, Q547L, L407A, and I417A) in an IC_{50} assay and related to WT h15-LOX-1.[22–24] As is observed in Table 4, **ML351** had an IC_{50} of 0.33 ± 0.02 μM against WT, with F414I being the only mutant manifesting a change in potency. F414I displayed an IC_{50} of 4.1 ± 1 μM, which was 12-fold less potent than WT, while F414W and E356Q showed little change in potency (IC_{50} values of 0.77 ± 0.1 and 0.87 ± 0.2 μM, respectively), in qualitative agreement with the docking results. Q547L, R404L, R402L, L407A, and I417A exhibited similar potency as WT, indicating minimal or no interaction with **ML351** (Table 4).

The second inhibitor screened, compound **18**, (4-(5-(Naphthalen-1-yl)-1,3,4-oxadiazol-2-ylthio)but-2-ynyl-4-naphthalene) is a derivative of **ML094**.[22] This molecule was chosen due to its lower potency than **ML094**, and thus did not require the Morrison equation for IC_{50} determination, simplifying data interpretation. Analysis of compound **18** data (Table 4) indicated that L407A had the largest effect on inhibition, with a greater than 1000-fold decrease in potency ($IC_{50} > 50$ μM). E356Q had a modest effect on the potency of compound **18** relative to WT ($IC_{50} = 0.14 \pm 0.04$ μM and 0.05 ± 0.001 μM, respectively), while Q547L exhibited no effect on potency (0.040 ± 0.01 μM). F414W also had a large change in potency relative to WT ($IC_{50} = 0.20 \pm 0.04$ μM), however F414I had little effect ($IC_{50} = 0.078 \pm 0.03$ μM). R404L, R402L and I417A had little or no effect on thepotency of compound **18** ($IC_{50} = 0.060 \pm 0.02$ μM, 0.050 ± 0.001 μM and 0.065 ± 0.01 μM, respectively).

Steady-State Inhibition Kinetics

Given the changes in IC_{50} values of these active site mutants, it was important to confirm these effects with steady-state enzyme inhibitor kinetics with the key mutants that exhibited the greatest effect on the IC_{50} value (F414I, F414W, E356Q, and L407A). AA was used as substrate with F414W, E356Q and L407A, while LA was used with F414I, due to product degradation, as previously discussed. The formation of 15-HpETE or 13-HpODE was monitored as a function of substrate and inhibitor concentration in the presence of 0.01% Triton X-100. Replots of K_M / k_{cat} and $1/ k_{cat}$ against inhibitor concentration produced linear plots from which K_{ic} (equilibrium constant of dissociation from the enzyme) and K_{iu} (equilibrium constant of dissociation from the enzyme substrate complex) were extracted (see relative values to WT, Table 5). The data were consistent with mixed inhibition, which is typical of LOX inhibitors.[24] All data were also plotted in the Dixon format (not shown), which confirmed the K_{ic} and K_{iu} for each mutant. It should be noted that the WT K_{ic} varies depending on the substrate used (AA vs. LA), possibly due to the allosteric site and hence the relative change in potency is shown.

As shown in Table 5, the K_{ic} of **ML351** for F414W was similar to WT, but the K_{ic} for F414I was 25-fold greater than WT (primary data are shown in the supplement, Table S1). These data suggest that F414 interacts directly with **ML351**, possibly in a manner analogous to the

interaction between F414 and the substrate (i.e. π-π stacking), with only the aromatic to aliphatic substitution significantly disrupting the π-πstacking and thus its binding.[27]

With regards to the **ML094** derivative, compound **18**, which contains a similar naphthalene moiety but a longer hydrophobic arm than **ML351**, mutations at F414 also affected binding of the inhibitor to the enzyme but in a different way. In this case, F414I did not have an effect on the K_{ic} of compound **18** relative to WT, exhibiting only a 1.6-fold decrease in potency (Table 5). However, F414W had a larger effect on K_{ic} relative to WT, decreasing the potency by 8.5-fold. This result suggests that changing F414 to the larger W414 impacts the binding of compound **18** but not **ML351**, which is a smaller molecule. On the other hand, F414I only decreased the potency slightly, supporting the hypothesis that sterical aspects are more important for compound **18** than aromaticity.

With respect to E356Q, the K_{ic} of **ML351** increases only 2-fold, suggesting minimal inhibitor interactions, consistent with the predicted docking pose. However, a 20-fold decrease in potency was observed for E356Q with compound **18** (Table 5) relative to WT. This result was not predicted by the docking calculations, although compound **18** was predicted to bind in a "flipped" orientation in E356Q. E356 is involved in the second coordination sphere of the active site iron, as seen in the soybean and rabbit 15-LOX-1 structures, therefore converting the Glu to a Gln could either affect a direct interaction with compound **18**, or the configuration of the second coordination sphere.[25,38]

The mutation L407A has little effect on the potency of **ML351**, but greater than 1000-fold decrease in potency for compound **18** ($IC_{50} > 50$ μM). Qualitatively, this result was expected based on the docking predictions, although the magnitude of the decrease in potency for compound **18** is dramatic, emphasizing the critical role of the L407 side chain in binding the U-shaped compound **18**. It should be noted that steady-state inhibition kinetics could not be performed with L407A due to the dramatic drop in potency (greater than 1000-fold) and hence our inability to reach high enough inhibitor concentrations due to solubility constraints.

Overall, the results support the models shown in Figure 1, in which both **ML351** and compound **18** bind with the naphthalene group in a deep hydrophobic pocket, with F414 lying at the end of the pocket. The mutations F414I and F414W, as well as L407A, have differing impacts on the two inhibitors due to compound **18** being approximately twice the size of **ML351**, which presents greater constraints on its possible binding modes. Q547L was predicted and confirmed to have little impact on binding of either inhibitor, consistent with the Gln side chain not being predicted to form hydrogen bonds with either inhibitor. The results with E356Q are more difficult to interpret. This charge-changing mutation had little impact on **ML351** but a significant negative effect on the K_{ic} of compound **18** (although the impact on the IC_{50} measurement was more modest).

Conclusions

These results have differing implications for improving the binding affinity of compounds in the **ML351** and **ML094** series (compound **18** being a member of the latter). Compound **18**

and other members of the **ML094** series are predicted to nearly completely fill the binding pocket, from the narrow constriction created by the side chain of Leu407 through the hydrophobic pocket terminating in Phe414. There may be modest opportunities to improve binding interactions in these regions, given these constraints, although the impact of E356Q may suggest opportunities to optimize electrostatic complementarity. By contrast, the much smaller **ML351** presents potentially significant opportunities for further optimization, although in practice this has proven to be challenging.[24] Two views of the predicted binding mode of **ML351** are shown in Figure 3, in which molecular surfaces emphasize key steric constraints. These views suggest that the challenge is to identify ways of extending the molecule into the narrow constriction formed by L407, while maintaining the hydrogen-bond of the oxazole to the ferric-water moiety. Our previously published SAR investigation increased the length of the methylamine, which improved potency slightly (compounds **21**, **22** and **23**); however, too long of an alkyl chain or a branched chain decreased potency (compounds **24** and **26**, respectively).[23,24] These data are consistent with our model where the alkyl chain would extend into the active site toward the cavity exit.[23,24] We also observed that modifying the oxazole ring or the cyano moiety lowered potency dramatically (compounds **33**–**40**), possibly due to disruption of the oxazole hydrogen-bond to the ferric-water moiety. Based on the model presented here, we are currently designing new inhibitors, such as substituting an alkyl moiety onto the oxazole, rather than the amine. The goal is to maintain the hydrogen-bond interaction with the Fe^{2+}-H_2O, while efficiently filling the open cavity off the alkyl amine to gain binding affinity and potency.

Acknowledgments

Abbreviations

LOX	lipoxygenase
h15-LOX-1	human reticulocyte 15-lipoxygenase-1
tPA	tissue plasminogen activator
FDA	Food and Drug Administration
s15-LOX-1	soybean 15-lipoxygenase-1
r15-LOX	rabbit reticulocyte 15-LOX
AA	arachidonic acid
12-HpETE	12-hydroperoxyeicosatetraenoic acid
LA	linoleic acid
9R-HpODE	9-(R)-hydroperoxyoctadecadienoic acid
13-HpODE	13-(S)-hydroperoxyoctadecadienoic acid

15-HpETE	15-hydroperoxyeicosatetraenoic acid
ICP-MS	inductively coupled plasma mass spectrometer
EDTA	ethylenediaminetetraacetic acid
BSA	bovine serum albumin
SDS-PAGE	sodium dodecyl sulfate poly-acrylamide gel electrophoresis
RMSD	root-mean-squared-distance

REFERENCES

1. Kuhn H, O'Donnell VB. Prog. Lipid Res. 2006; 45:334. [PubMed: 16678271]

2. Nasjletti A. Hypertension. 1998; 31:194. [PubMed: 9453302]

3. Chawengsub YG, Campbell WB. Am. J. Physiol. Heart Circ. Physiol. 2009; 297:H495. [PubMed: 19525377]

4. Zhu D, Ran Y. Physiol. Sci. 2012; 62:163.

5. Belkner JS, Kuhn H. J. Biol. Chem. 1998; 273:23225. [PubMed: 9722553]

6. Pirillo A, Uboldi P, Kuhn H, Catapano AL. Biochim. Biophys. Acta. 2006; 1761:292. [PubMed: 16647293]

7. Folcik VA, Nivar-Aristy RA, Krajewski LP, et al. J. Clin. Invest. 1995; 96:504. [PubMed: 7615823]

8. Pidgeon GP, Lysaght J, Krishnamoorthy S, et al. Cancer Metastasis Rev. 2007; 26:503. [PubMed: 17943411]

9. Klil-Drori AJ, Ariel A. Prostag. Other Lipid Mediat. 2013; 106:16.

10. Laybutt DR, Sharma A, Sgroi DC, Gaudet J, Bonner-Weir S, Weir GC. J. Biol.Chem. 2002; 277:10912. [PubMed: 11782487]

11. Sears DD, Miles PD, Chapman J, Ofrecio JM, Almazan F, Thapar D, Miller YI. PLoS One. 2009; 4:e7250. [PubMed: 19787041]

12. Dobrian A, Ma Q, Lindsay JW, Cole BK, Ma K, et al. Biochem. Biophys. Res. Commun. 2010; 403:485. [PubMed: 21094135]

13. van Leyen K. CNS Neurol. Disord. Drug Targets. 2013; 12:191. [PubMed: 23394536]

14. van Leyen K, Kim HY, Lee SR, Jin G, Arai K, Lo EH. Stroke. 2006; 37:3014. [PubMed: 17053180]

15. van Leyen K, Arai K, Jin G, Kenyon V, Gerstner B, Rosenberg PA, Holman TR, Lo EH. J. Neurosci. Res. 2008; 86:904. [PubMed: 17960827]

16. Weinstein DS, Gu Z, Langevine C, Ngu K, Fadnis L, et al. Bioorg. Med. Chem. Lett. 2005; 15:1435. [PubMed: 15713402]

17. Ngu KW, Liu W, Langevine C, Combs DW, Zhuang S, Chen X, Madsen CS, Harper TW, Ahmad S, Robl J. Bioorg. Med. Chem. Lett. 2011; 21:4141. [PubMed: 21696952]

18. Weinstein DS, Ngu K, Langevine C, Combs DW, Zhuang S, Chen C, Madsen CS, Harper TW, Robl JA. Bioorg. Med. Chem. Lett. 2007; 17:5115. [PubMed: 17656086]

19. Pelcman B, Sanin A, Nilsson P, No K, Schaal W, Olofsson CK-J, et al. Bioorg. Med. Chem. Lett. 2015; 25:3017. [PubMed: 26037319]

20. Pelcman B, Sanin A, Nilsson P, No K, Schaal W, Ohrman S, et al. Bioorg. Med. Chem. Lett. 2015; 25:3024. [PubMed: 26037322]

21. Eleftheriadis N, Thee S, Biesebeek J, van der Wouden P, Baas B-J, Dekker FJ. Eur. J. Med. Chem. 2010; 94:265.

22. Rai G, Kenyon V, Jadhav A, Schultz L, Armstrong M, Jameson B, Hoobler E, Leister W, Simeonov A, Holman TR, Maloney DJ. J. Med. Chem. 2010; 53:7392. [PubMed: 20866075]

23. Rai G, Joshi N, Perry S, Yasgar A, Schultz L, et al. Probe Reports from the NIH Molecular Libraries Program. 2010

24. Rai G, Joshi N, Jung JE, Liu Y, Schultz L, et al. J. Med. Chem. 2014; 57:4035. [PubMed: 24684213]

25. Gillmor SA, Villasenor A, Fletterick R, Sigal E, Browner MF. Nat. Struct. Biol. 1997; 4:1003. [PubMed: 9406550]

26. Choi J, Chon JK, Kim S, Shin W. Proteins. 2008; 70:1023. [PubMed: 17847087]

27. Gan Q, Sloane DL, Sigal E. J. Biol. Chem. 1996; 271:25412. [PubMed: 8810309]

28. Klinman JP. Acc. Chem. Res. 2007; 40:325. [PubMed: 17474709]

29. Borngraber S, Anton M, Kuhn H. J. Mol. Biol. 1996; 264:1145. [PubMed: 9000636]

30. Sloane DL, Barnett J, Sigal CS. Protein Eng. 1995; 8:275. [PubMed: 7479689]

31. Sloane DL, L R, Craik CS, Sigal E. Nature. 1991; 354:149. [PubMed: 1944593]

32. Amagata T, Johnson TA, Stessman CC, Loo CP, Lobkovsky E, Clardy J, Crews P, Holman TR. J. Nat. Prod. 2003; 66:230. [PubMed: 12608855]

33. Schrodinger Release 2014-1: Maestro, ver. 9.7. New York, NY: Schrodinger, LLC; 2014.

34. Xu S, Mueser TC, Marnett LJ, Funk MO. Structure. 2012; 20:1490. [PubMed: 22795085]

35. Kobe MJ, Mitchell CE, Bartlett SG, Newcomer ME. J. Biol. Chem. 2014; 289:8562. [PubMed: 24497644]

36. Armstrong MM, Freedman CJ, Jung JE, Zheng Y, Kalyanaraman C, Jacobson MP, Simeonov A, Maloney DJ, van Leyen K, Jadhav A, Holman TR. Bio. Med. Chem. 2016; 24:1183.

37. Eleftheriadis N, Neochoritiz CG, Leus NGJ, van der Wouden PE, Dömling A, Dekker FJ. J. Med. Chem. 2015; 58:7850. [PubMed: 26331552]

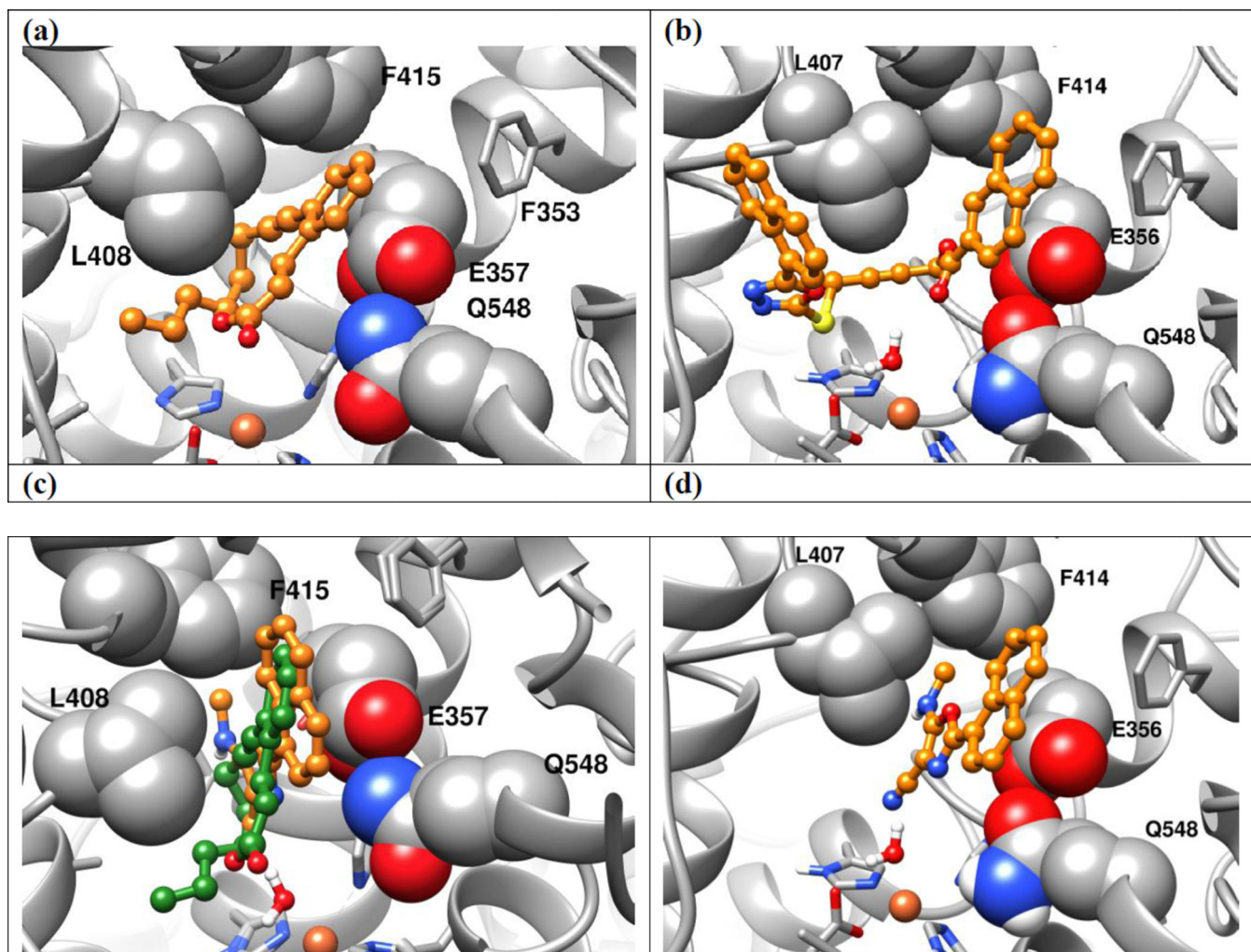38. Tomchick DR, Cymborowski M, Minor W, Holman TR. Biochemistry. 2001; 40:7509. [PubMed: 11412104]

Author Manuscript

Author Manuscript

Author Manuscript

Author Manuscript

Figure 1.
(a) Rabbit 15-LOX and RS75091 inhibitor from the crystal structure (pdb ID: 2P0M, chain B), (b) docking pose of compound **18** docked to Human 15-LOX model, (c) docking pose of **ML351** to human 15-LOX model shown in (d) is superimposed on the rabbit 15-LOX structure (pdb ID: 2P0M, chain B), and (d) docking pose of **ML351** docked to Human 15-LOX. The **ML351** binding modes shown in figures (c) and (d) are identical. The inhibitor is shown in ball-and-stick representation and Fe^{2+} ion is shown in sphere representation. Carbon, nitrogen and oxygen atoms of the inhibitors are shown in orange, blue and red colors respectively. Fe^{2+} ion is shown in orange color. In figure (c) carbon atoms of the inhibitor RS7509 are shown in green color. Protein residues mutated in this study are shown in sphere representation. Carbon, nitrogen and oxygen atoms of the protein are shown in gray, blue and red colors respectively. It should also be noted that the rabbit 15-LOX amino acid numbering is one greater than that of human 15-LOX due to an amino acid insertion early in the sequence.
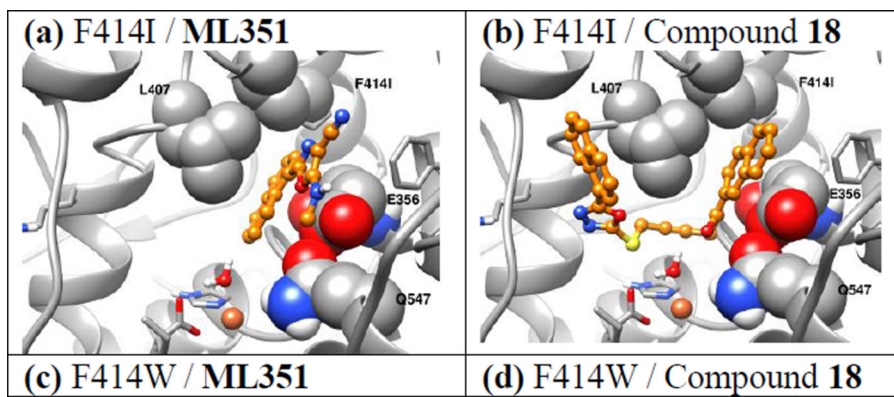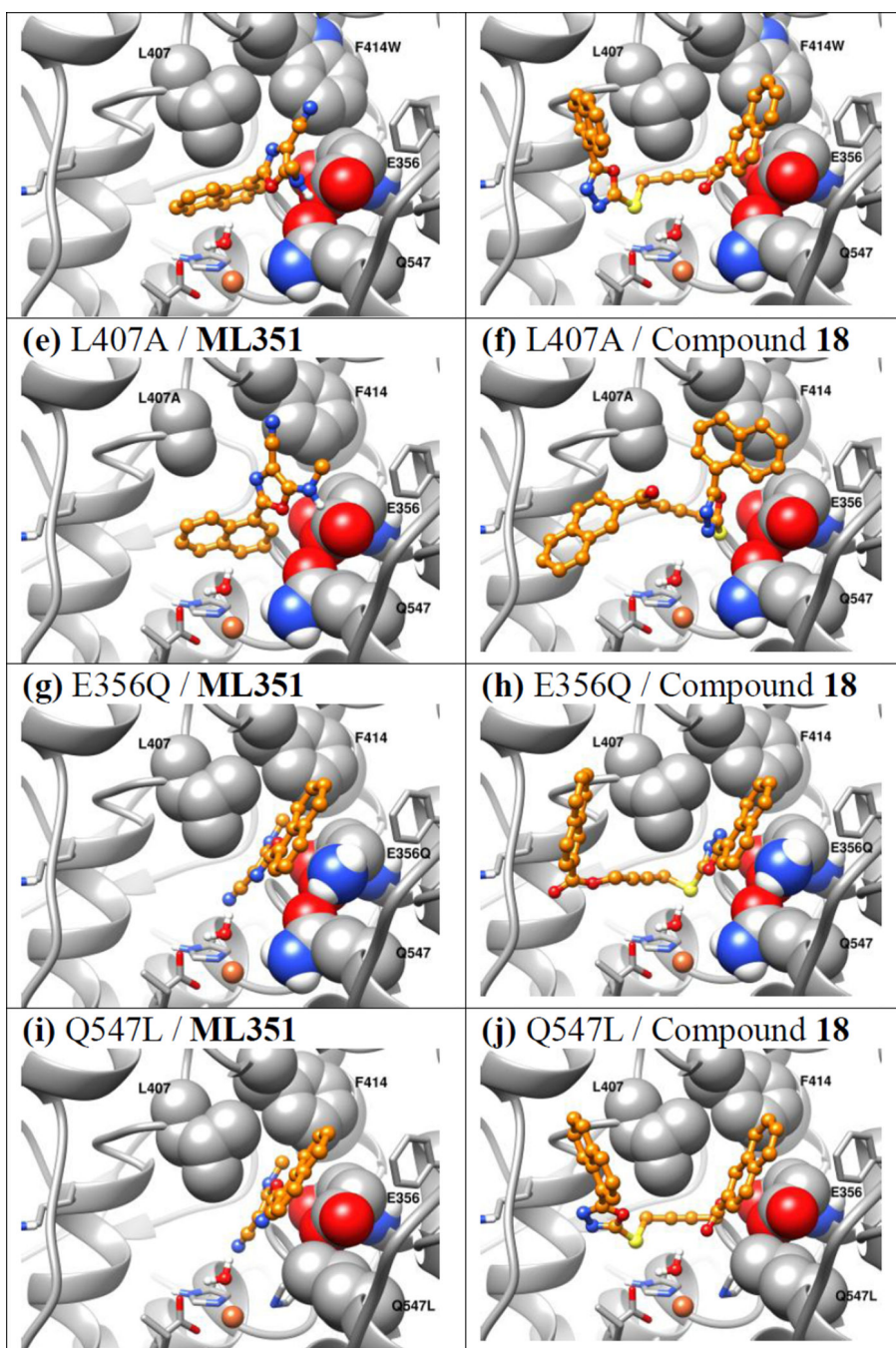
Figure 2.
Docking pose of inhibitors **ML351** and compound **18**, docked to F414I (a, b), F414W (c, d), L407A (e, f), E356Q (g, h), and Q547L (i, j) human 15-LOX-1 model. Active site residues subjected to mutation are shown in sphere representations. Inhibitors are shown in ball-and-stick representation (carbon, nitrogen, oxygen and sulfur atoms are shown in orange, blue, red and yellow color). Fe^{2+} ion is shown orange color and the water molecule is shown in ball-and-stick representation. Due to the effect of mutation, the lowest energy docking pose of the inhibitors for each mutant are different from the WT docking pose.
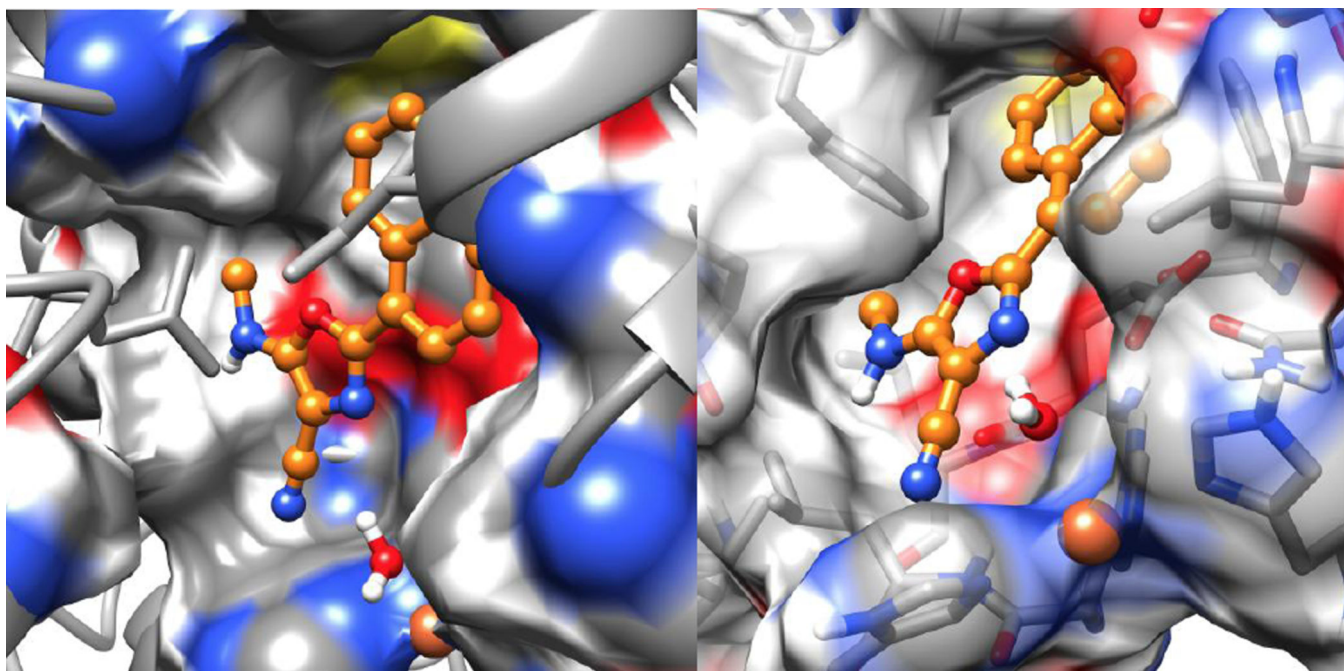
Figure 3.
Docking pose of **ML351** to the human 15-LOX-1 model shown in two different views, with electrostatic van der Waals boundaries in the active site. **ML351** is shown ball-and-stick representation. Carbon and oxygen atoms of **ML351** are shown orange and red colors respectively. Carbon, nitrogen and oxygen atoms of the protein residues are shown in gray, blue and red colors respectively.

Table 1
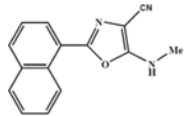
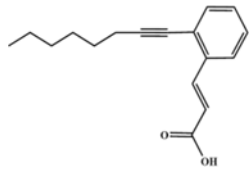Chemical structures and identification numbers of inhibitors.

INHIBITOR STRUCTURE	INHIBITOR ID#
	ML351
	Compound 18
	ML094
	RS75091

Table 2

Glide-XP docking scores and heavy atom root-mean-square distance (RMSD) between the docked poses of inhibitors **18** and **ML351**, docked against WT h15-LOX-1and mutants.

Protein	ML351			18		
	XP Docking	Heavy atom RMSD (Å)	XP Score-in-Place	XP Docking	Heavy atom RMSD (Å)	XP Score-in-Place
WT	−5.2	-	−5.2	−10.2	-	−10.2
F414I	**−4.7**	**6.6**	−5.1	−9.4	1.4	−9.2
F414W	−6.9	6.7	−5.5	**−8.7**	**1.9**	−10.1
L407A	−5.7	6.5	4.4	**−8.4**	**8.3**	−8.4
E356Q	−7.3	0.2	−7.3	**−11.1**	**8.1**	−11.7
Q547L	−5.2	0.2	−5.4	−10.3	0.3	−9.9

Table 3

Steady-state kinetic parameters of mutants that exhibited the greatest change in potency relative to WT h15-LOX-1.

		K_M	k_{cat}	k_{cat}/K_M	% Metallation
AA*	WT	8.8 (0.8)	11 (0.5)	1.3 (0.06)	50
	Q547L	11 (1)	2.9 (0.1)	0.3 (0.01)	59
	E356Q	4.1 (0.4)	3.0 (0.1)	0.7 (0.04)	42
	F414W	6.5 (0.6)	2.8 (0.08)	0.4 (0.02)	52
	F414I	11 (0.7)	1.8 (0.05)	0.2 (0.006)	57
	L407A	5.5 (1)	2.5 (0.2)	0.45 (0.01)	75
LA*	WT	7.7 (0.8)	11 (0.4)	1.5 (0.09)	50
	F414I	6.1 (0.2)	1.6 (0.03)	0.3 (0.007)	57

*The substrate used is indicated on the left and the error in parentheses.

Table 4

IC$_{50}$ values (μM) of WT h15-LOX-1 and mutants against **ML351** and compound **18**.

Enzyme	ML351	18
WT	0.33 ± 0.02	0.050 ± 0.001
F414I	4.1 ± 1	0.078 ± 0.03
F414W	0.77 ± 0.1	0.20 ± 0.04
E356Q	0.87 ± 0.2	0.14 ± 0.04
Q547L	0.30 ± 0.06	0.040 ± 0.01
R404L	0.26 ± 0.09	0.060 ± 0.02
R402L	0.12 ± 0.01	0.050 ± 0.001
L407A	0.39 ± 0.01	> 50
I417A	0.18 ± 0.08	0.065 ± 0.01

Table 5

The x-fold decrease in potency (inhibitor constant (K_{ic})) of **ML351** and compound **18** with the LOX mutants, relative to WT h15-LOX-1.

	ML351	18
WT	1	1
F414I	25	1.6
F414W	1	8.5
E356Q	2	20
L407A	1	>1000